Available online at www.sciencedirect.com
SCIENCE DIRECT®
ELSEVIER
Nuclear Instruments and Methods in Physics Research B 233 (2005) 125–131
NIM B
Beam Interactions with Materials & Atoms
www.elsevier.com/locate/nimb

Spin-dependent correlated electron emission from ordered and disordered materials

J. Berakdar [a,*], A. Ernst [a], K.A. Kouzakov [b]

[a] *Max-Planck Institut für Mikrostrukturphysik, Weinberg 2, D-06120 Halle, Germany*
[b] *Department of Physics, Moscow State University, Moscow 119992, Russia*

Available online 20 April 2005

Abstract

We study theoretically the spin-dependent electron–electron scattering in ordered and disordered magnetic surfaces. With the aid of the screened Korringa–Kohn–Rostocker (KKR) method and the density functional theory within the local-density approximation we calculate the spin-dependent Kohn–Sham crystal potential in which two excited electrons are propagating. The electronic band structure is also calculated and it is shown that a coincident measurement of two excited electrons from a magnetic surface gives access to the spin-resolved spectral distribution of the band electrons. We also discuss the case of disordered metals and point out the conditions under which the electronic spectral properties of the surface can be imaged by means of coincident electron measurements.

PACS: 79.20.Kz; 75.25.+z; 71.20.Be; 71.23.−k

Keywords: Magnetic surfaces; Spin-polarized electrons; KKR method; Binary alloys

1. Introduction

Substantial theoretical and experimental efforts are currently devoted to the investigation of magnetic systems, in particular those with a reduced dimensionality, such as surfaces and thins films [1,2]. These studies are motivated by the importance of these materials both from a fundamental and a technological point of view. The present work focuses on one aspect of quantum theory of magnetism, namely on the spin-dependent electron scattering and electron pair emission from ferromagnetic surfaces and binary alloys. A well-known technique related to the present study is the spin-polarized electron energy loss spectroscopy (SPEELS) which has been employed to

* Corresponding author. Tel.: +49 345 5582666; fax: +49 345 5511223.
E-mail addresses: jber@mpi-halle.de (J. Berakdar), aernst@mpi-halle.de (A. Ernst), kouzakov@srd.sinp.msu.ru (K.A. Kouzakov).

0168-583X/$ - see front matter © 2005 Published by Elsevier B.V.
doi:10.1016/j.nimb.2005.03.094

investigate the elementary (magnetic) neutral excitations of ferromagnets [3–6]. In SPEELS one measures the probability for an incident spin-polarized electron to loose certain amount of energy ΔE and momentum $\Delta\mathbf{k}$. If $\Delta\mathbf{k}$ and ΔE are sufficiently high a second electron may be emitted which in principle can be detected in coincidence with the scattered (primary) electron. As shown below the coincidence spectra of this electron pair can be utilized to study the spin-dependent collisions at surfaces and to map out the electronic structure of clean solids and binary alloys.

2. Spin-dependent electron scattering from clean surfaces

The two electrons emitted from a clean ordered surface obey the energy and wave vector balances

$$E_0 + E = E_e + E_s, \quad \mathbf{k}_{0,\|} + \mathbf{k}_\| + \mathbf{g}_\| = \mathbf{k}_{e,\|} + \mathbf{k}_{s,\|}. \tag{1}$$

Here, E is the energy of the valence band electron and $\mathbf{k}_\|$ is its (surface) Bloch wave vector. The surface reciprocal lattice vector is denoted by $\mathbf{g}_\|$. The energies of the incoming, the scattered and emitted vacuum electrons are respectively denoted by E_0, E_s, E_e and their surface-parallel wave vector components are $\mathbf{k}_{0,\|}$, $\mathbf{k}_{s,\|}$, $\mathbf{k}_{e,\|}$. All these quantities are supposed to be determined experimentally. Thus, the values of E and $\mathbf{k}_\|$ can be deduced from Eq. (1). There are various sources for the spin dependence of the electron scattering in solids, most notably exchange scattering and spin–orbit coupling (SOC). Here we are only concerned with systems where SOC is negligible (this can be checked experimentally [7,8]) and focus on effects due to the exchange interaction only. In addition, the experiments are currently not capable of resolving the final-state electron spin projections. Experimentally one measures, for a certain magnetization direction $\mathbf{M}$, denoted by $\Downarrow$, a spin asymmetry $\mathscr{A}$. This is done by registering the normalized difference $\mathscr{A}$ in the electron pair emission rate W for antiparallel and parallel alignment of the polarization vector of the incoming beam with $\mathbf{M}$, i.e. one determines

$$\mathscr{A}(\mathbf{k}_s, \mathbf{k}_e; \mathbf{k}_0) = \frac{W(\uparrow\Downarrow) - W(\downarrow\Downarrow)}{W(\uparrow\Downarrow) + W(\downarrow\Downarrow)}. \tag{2}$$

Theoretically $\mathscr{A}$ can be related to the spin asymmetry in the surface Bloch spectral functions as follows [7,8]

$$\mathscr{A}(\mathbf{k}_s, \mathbf{k}_e; \mathbf{k}_0) = P_e \sum_{l,\mathbf{g}_\|} \mathscr{A}_l^{(m)} \mathscr{A}_{l,\mathbf{g}_\|}^{(s)}. \tag{3}$$

Here, the atomic layers parallel to the surface are indexed by l and P_e is the magnitude of the polarization vector of the incoming beam. The projection of the projectile electron's spin parallel (antiparallel) to $\Downarrow$ is denoted by $\downarrow$ ($\uparrow$). $\mathscr{A}^{(m)}$ contains the information on the *sample's magnetic asymmetry*

$$\mathscr{A}_l^{(m)} = \frac{A(\mathbf{k}_\|, l, E, \Downarrow) - A(\mathbf{k}_\|, l, E, \Uparrow)}{A(\mathbf{k}_\|, l, E, \Downarrow) + A(\mathbf{k}_\|, l, E, \Uparrow)}, \tag{4}$$

where $A(\mathbf{k}_\|, l, E, \Uparrow)$ and $A(\mathbf{k}_\|, l, E, \Downarrow)$ are the Bloch spectral functions of respectively the majority and the minority band. Details of the scattering dynamics are encompassed in the *exchange scattering asymmetry* $\mathscr{A}^{(s)}$. As shown in [7,8], $\mathscr{A}^{(s)}$ tends to unity under a certain arrangement of the experimental setup in which case the magnetic asymmetry $\mathscr{A}_l^{(m)}$ in the spectral function can be measured. Details of the calculations of the sample's valence electron spectral function are given below.

3. Pair emission from disordered binary alloys

In this section we outline the theoretical treatment of the electron pair emission from a substitutionally disordered binary alloy A_xB_{1-x} that consists of two atomic components A and B with concentration $c_A = x$ and $c_B = 1 - x$. The condition $c_A + c_B = 1$ ensures full randomness, i.e. there is no statistical correlation in the lattice sites occupation. In addition we employ the single-site approximation, i.e. the one-electron potential at the lattice site j depends only on the occupation at j (by A or B atom). The crystal potential V_s is then expanded as a sum $V_s = \sum_j V_s^j$ of muffin–tin potentials V_s^j located at the sites j. The occupation indices ξ^j are random numbers taking the values $\xi^j = 1$ if the site j occupied by the atom of type A

and $\xi^j = 0$ otherwise. The on-site potentials are written as

$$V_s^j = \xi^j V_s^{j\mathrm{A}} + (1-\xi^j) V_s^{j\mathrm{B}}. \tag{5}$$

The configurational average $\langle \xi^j \rangle$ of ξ^j (hereafter we use the angle brackets $\langle \cdots \rangle$ for configurationally averaged quantities) is given by the probability that the atom A occupies the site j, i.e. $\langle \xi^j \rangle = x$ and x is the concentration of A. A relatively easy way of treating disordered alloys is the so-called virtual crystal approximation (VCA). In VCA the potential V_s^j is approximated as (5)

$$V_s^j = x V_s^{j\mathrm{A}} + (1-x) V_s^{j\mathrm{B}}, \tag{6}$$

and the calculations are performed in the same manner as for ordered clean surfaces, however using the potential (6). The second step in sophistication is the average t-matrix approximation (ATA) in which a configurational average is performed upon accounting for multiple scattering from $V_s^{j\mathrm{A/B}}$, i.e. one operates with t-matrices $t^{j\mathrm{A/B}}$ rather than with single scattering potentials. Obviously VCA becomes legitimate when V_s^j scatters only weakly or/and at higher energies, in both cases multiple scattering becomes less important. The coherent potential approximation (CPA) supersedes ATA in that the calculations are performed self-consistently, a fact which is particularly important for accurate calculations of ground state properties, for a detailed discussion of this issue we refer to [9–14].

In the case of fast projectile electrons (~30 keV) traversing a thin standing film one can perform the experiment under certain conditions where the electron–electron scattering is the important factor, i.e. one neglects final and initial (vacuum) electron scattering events from the crystal [15,16]. The measured quantity is a cross section $W(E_s, \Omega_s, E_e, \Omega_e)$ which is differential in the solid emission angles of two electrons Ω_e and Ω_s and in their energies E_s, E_e. The configurational average of $W(E_s, \Omega_s, E_e, \Omega_e)$ is [17]

$$\langle W(E_s, \Omega_s, E_e, \Omega_e) \rangle = \frac{k_s k_e}{(2\pi)^3 k_0} \left(\frac{\mathrm{d}\sigma}{\mathrm{d}\Omega} \right)_{ee} \langle A(\mathbf{k}, E) \rangle. \tag{7}$$

Here $\left(\frac{\mathrm{d}\sigma}{\mathrm{d}\Omega}\right)_{ee}$ is the Mott cross section. Thus, the cross section yields direct information on the spectral density of disordered samples. It should be noted in this context that, due to the high incident electron energy, this technique provides information on the bulk electronic structure. Correspondingly the theory employs the bulk spectral function. If the spin polarization of the incoming electron is known then the asymmetry in the bulk spin-spectral density can be measured by measuring the spin asymmetry, as given by Eq. (2). This kind of experiments have not been yet done.

In general, the electron pair emission is strongly influenced by scattering from the crystal [18,19]. In addition, at low and moderate energies ($\leqslant$1 keV) only the first few atomic layers are relevant for the electron pair emission process [8,16]. In this general case the theoretical treatment is as follows. At first the operator $M(\mathbf{k}_s, \mathbf{k}_0)$ describing the interaction of the incoming electron (incident with a wave vector $\mathbf{k}_0$ and leaving the sample with the wave vector $\mathbf{k}_s$) with the sample is written as a sum over the lattice sites $M(\mathbf{k}_s, \mathbf{k}_0) = \sum_j M_j(\mathbf{k}_s, \mathbf{k}_0)$, where

$$M_j(\mathbf{k}_s, \mathbf{k}_0) = \left\langle \mathbf{k}_s \middle| V_s^j g_s^+ W_{se} + W_{se} g_0^+ V_s^j \middle| \mathbf{k}_0 \right\rangle. \tag{8}$$

Here W_{se} is the interaction potential between the primary and the secondary electrons and $g_s^+(g_0^+)$ is the retarded crystal (free) Green's function. From Eq. (5) follows then that

$$M_j(\mathbf{k}_s, \mathbf{k}_0) = \xi^j M_{j\mathrm{A}}(\mathbf{k}_s, \mathbf{k}_0) + (1-\xi^j) M_{j\mathrm{B}}(\mathbf{k}_s, \mathbf{k}_0). \tag{9}$$

With these equations the cross section is expressed as

$$W(E_s, \Omega_s, E_e, \Omega_e) = \frac{k_s k_e}{(2\pi)^5 k_0} \sum_{jj'} \left\langle \chi_{\mathbf{k}_e} \middle| M_j(\mathbf{k}_s, \mathbf{k}_0) A(E) M_{j'}^\dagger(\mathbf{k}_s, \mathbf{k}_0) \middle| \chi_{\mathbf{k}_e} \right\rangle, \tag{10}$$

where $\chi_{\mathbf{k}_e}$ is the wave function of the secondary (vacuum) electron. The one-electron spectral function $A(E)$ derives from the occupied single-electron (Kohn–Sham) orbitals according to $A(E) = \sum_{i_{\mathrm{occ}}} |\chi_i\rangle\langle\chi_i| \delta(E - \varepsilon_i) = -\frac{1}{\pi} \mathrm{tr} \Im G(\mathbf{k}, \mathbf{k}', E)$, where $G(\mathbf{k}, \mathbf{k}', E)$ is the retarded single-particle Green's function of the band electrons. By carrying out the configurational average of the cross section (10) one finds [17] that the disorder-averaged cross

section is composed of a coherent and an incoherent terms $\langle W(E_s,\Omega_s,E_e,\Omega_e)\rangle = \langle W^{coh}(E_s,\Omega_s,E_e,\Omega_e)\rangle + \langle W^{incoh}(E_s,\Omega_s,E_e,\Omega_e)\rangle$, where

$$\left\langle W^{coh}(E_s,\Omega_s,E_e,\Omega_e)\right\rangle = \frac{k_s k_e}{(2\pi)^5 k_0}\sum_{jj'}\left\langle \langle\chi_{\mathbf{k}_e}|\langle M_j\rangle A(E)\langle M_{j'}^{\dagger}\rangle|\chi_{\mathbf{k}_e}\rangle\right\rangle, \quad (11)$$

and

$$\left\langle W^{incoh}(E_s,\Omega_s,E_e,\Omega_e)\right\rangle = \frac{k_s k_e}{(2\pi)^5 k_0}\sum_{j}\left\{x\left\langle \langle\chi_{\mathbf{k}_e}|M_{jA}A(E)M_{jA}^{\dagger}|\chi_{\mathbf{k}_e}\rangle\right\rangle + (1-x)\left\langle \langle\chi_{\mathbf{k}_e}|M_{jB}A(E)M_{jB}^{\dagger}|\chi_{\mathbf{k}_e}\rangle\right\rangle - \left\langle \langle\chi_{\mathbf{k}_e}|\langle M_j\rangle A(E)\langle M_j^{\dagger}\rangle|\chi_{\mathbf{k}_e}\rangle\right\rangle\right\}. \quad (12)$$

$\langle W^{coh}\rangle$ and $\langle W^{incoh}\rangle$ are due to the coherent and incoherent scattering from the crystal potential. From Eqs. (8) and (9) follows that $\langle M_j(\mathbf{k}_s,\mathbf{k}_0)\rangle = xM_{jA}(\mathbf{k}_s,\mathbf{k}_0) + (1-x)M_{jB}(\mathbf{k}_s,\mathbf{k}_0)$. Having derived the basic formal equations for evaluating the cross sections we mention now some numerical details of the calculations. In short, the electronic band structure is dealt with on the basis of CPA whereas due to their higher energies (compared to the Fermi energy ε_F) the excited (vacuum) electrons are treated with VCA. The single-site scattering potentials are evaluated from a self-consistent density-functional theory (within local-density approximation, LDA). The total crystal potential consists of a muffin–tin sum over these single-site potentials. The scattering matrix elements are then evaluated numerically.

4. Electronic band structure as a multiple scattering problem

To provide the self-consistent potentials and the scattering matrices we used the Korringa–Kohn–Rostoker (KKR) Green's function method [20,21] within the density functional theory (DFT) which is rooted in multiple scattering theory. The KKR method is naturally designed to study systems with randomness because it supplies explicitly the one-electron Kohn–Sham Green function needed in the coherent potential approximation (CPA) method [22]. The KKR is also advantageous in that it separates effects related to purely geometric aspects of the crystal lattice (positions of atoms) from the dynamics of the particular atoms constituting the material. Each value of the energy and crystal momentum is dealt with directly and independently without recourse to a variational principle and without the need for orthogonalization. For any (non-interacting) ensemble of atoms the scattering operator $T(E)$ is written in terms of single-site t-matrices or so-called scattering path operator (for a generalization to interacting systems see [25])

$$T(E) = \sum_n t^n(E) + \sum_{n\neq m} t^n(E)G^0(E)t^m(E) + \cdots = \sum_{nm}\tau^{nm}, \quad (13)$$

$$[\tau(E)]^{nm}_{LL'} = \{[t^n_l(E)]^{-1} - g^{nm}_{LL'}(E)\}^{-1}. \quad (14)$$

Here $g(E)$ is the structure constants representing the free-electron Green function. The relation (14) is the central equation of the KKR method.

In our realization of the KKR method the crystal potential and charge density are constructed within the Wigner–Seitz cell including non-spherical contributions and near-field correction according to [23]. We apply typically maximal angular momentum $l_{max} = 3$ for the valence states and $l_{max} = 6$ for the potential and density representations, respectively. For the k-integration we used a special point method [24] with 256 points in the irreducible Brillouin zone.

5. Results and interpretations

For the ordered three dimensional systems, Eq. (14) is readily solved at the energy E and for the wave vector $\boldsymbol{k}$ in the first Brillouin zone of the reciprocal lattice. In this case the size of the KKR matrix is determined by the restricted size of the unit cell which makes the computations rather efficient. Systems with a broken translational symmetry such as clusters, impurities and alloys are treated within the real-space multiple scattering theory. However, solving the KKR equation is limited by the size of the matrix equation (14) which can be very large for realistic materials.

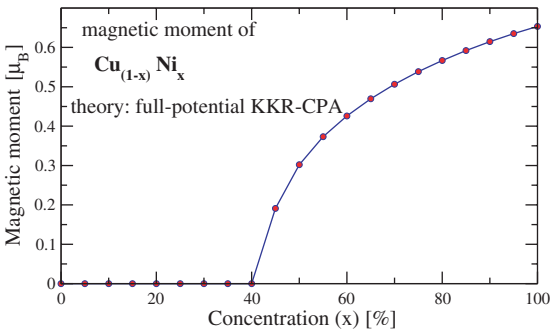

Fig. 1. The magnetic moment in Bohr magneton of the binary alloy $Cu_{(1-x)}Ni_x$ as a function of the concentration x. Calculations are performed using the KKR-CPA.

For random substitutional alloys the problem is simplified by the fact that the crystal is periodic, however the distribution of the atoms is random. All three methods, VCA, ATA, CPA-KKR [9–11,13] have been realized numerically. Here we discuss briefly some typical results of the calculations. Fig. 1 demonstrates how the value of the magnetic moment of the binary alloy $Cu_{(1-x)}Ni_x$ is governed by varying the dopant concentration x. The electron pair emission is capable of tracing this change by performing a spin-asymmetry measurement according to Eq. (2) and extracting under the appropriate geometry [7,8] the magnetic spin asymmetry of the sample according to relation (4). A detailed information is obtained by conducting the measurement under the condition where Eq. (7) applies (i.e. transmission mode, high incident energies and where binary electron–electron collision is dominant). As clear from Eq. (7) the measured cross section is readily related to the configurational average of the spectral function (the Mott cross section is known analytically). Fig. 2 shows typical results of $\langle A \rangle$ for Cu_xNi_{1-x} as a function of the surface-parallel wave vector components at a fixed binding energy $E = \varepsilon_F$ (i.e. we perform a Fermi-surface mapping). We note the (full potential) self-consistent results of Fig. 2 agree qualitatively with previous non-self consistent calculations [10]. The characteristics of the Fermi surface are markedly changed with an increase of the Ni concentration. For Cu it shows

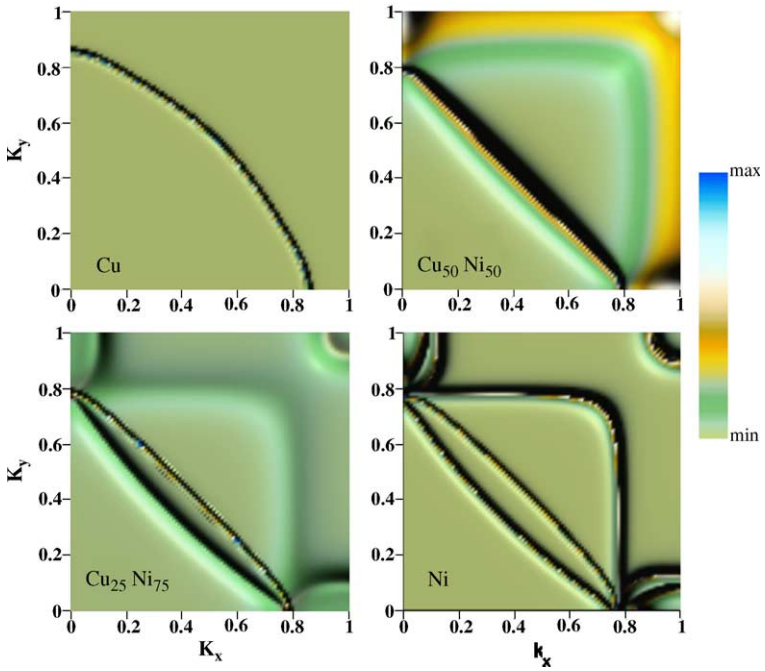

Fig. 2. Fermi-surface map of $Cu_{x-1}Ni_x$ system in (001) plane calculated within the KKR-CPA. The components of the wave vectors are given in units of $2\pi/a$, where a is the lattice constant.

a onefold, electron-like behaviour whereas for Ni a manyfold, electron-like with hole pockets is evident. The spin-splitting of the 3*d* Fermi surface of Ni diminishes at roughly $x = 0.5$ which is also clear from Fig. 1.

Relation (7) connects the measured cross section with the sample electronic structure. This direct connection is generally not valid. For example when lowering the energies or operating in the reflection mode the electron–crystal scattering becomes a key factor. An example is shown in Fig. 3 for a 200 eV electron incident normal to the surface of $Cu_{(1-x)}Ni_x$ and back reflected under 45° with respect to the surface normal $\hat{\mathbf{n}}$. The secondary electron is emitted under 90° with respect to the primary electron and 45° relative to $\hat{\mathbf{n}}$. The electron wave vectors and $\hat{\mathbf{n}}$ are in the same plane. What is considered is the sharing within the electron pair of the total energy $E_{tot} = E_s + E_e$. The band structure is evaluated via KKR-CPA and the scattering states are described by means of VCA. The various peaks seen in Fig. 3 are the results of the pair diffraction [18] involving the reciprocal lattice vectors $\mathbf{g}_{\parallel} = (00)$ and $\mathbf{g}_{\parallel} = \pm(1\,1)$, and also due to the crossing of the Fermi surface in the (001) plane. In this case the incoherent scattering contribution as given by Eq. (12) is of a less relevance due to the similar scattering properties of Ni and Cu sites. This situation changes when the constituent atoms of the binary alloy scatter differently (cf. Fig. 4). This is demonstrated by considering Al-based binary alloys. For a clean aluminum ($x = 1$) one observes in Fig. 4 a structure in the region $0.5 > |(E_s - E_e)/E_{tot}|$ and two structures in the regions $1 \geqslant |(E_s - E_e)/E_{tot}| > 0.5$ which correspond respectively to the electron pair diffraction with the reciprocal lattice vectors $\mathbf{g}_{\parallel} = (00)$ and $\mathbf{g}_{\parallel} = \pm(1\,1)$. The contribution of W^{incoh} is marginal for $Al_{0.85}Mg_{0.15}$ since the difference between the on-site muffin–tin potentials of the constituents is small. However in the case of $Al_{0.9}Li_{0.1}$ and especially $Al_{0.985}Pb_{0.015}$ the large difference between the on-site muffin–tin potentials induces a strong incoherent scattering of the electron pair in which case the energy sharing distribution is modified qualitatively by the incoherent scattering.

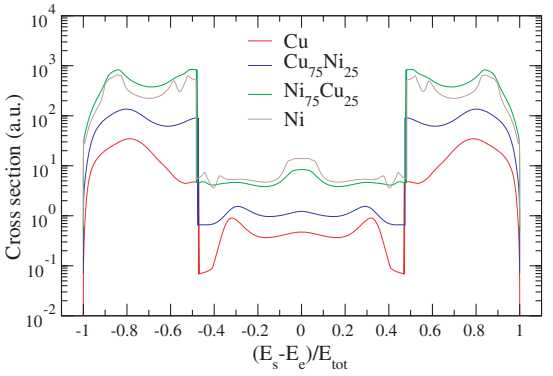

Fig. 3. The energy sharing distribution at an incidence energy $E_0 = 200$ eV from the (001) face of a copper–nickel alloy. The sum energy of the electrons is such that the emitted electron originates from the Fermi level (cf. Eq. (1)), the polar angles are $\theta_s = \theta_e = 45^{\circ}$ with respect to the [001] direction.

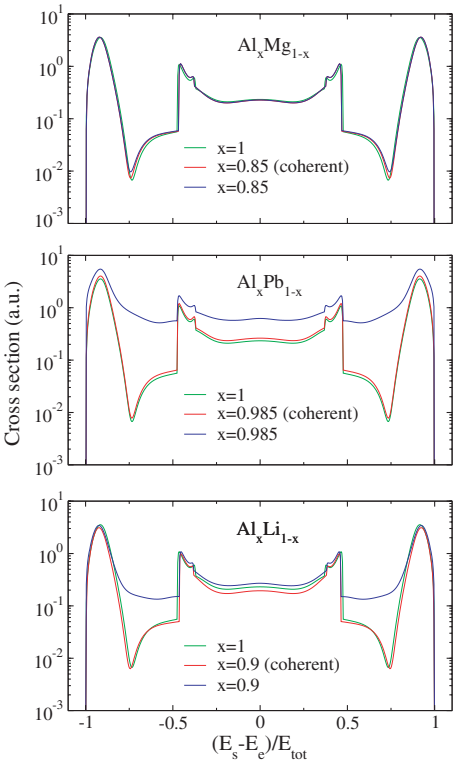

Fig. 4. Same geometrical arrangement as in Fig. 3. The electron pair is emitted from the Fermi level and from the (001) face of the aluminum alloy indicated in the figures.

6. Conclusions

In this work we described briefly the spin-dependent electron pair emission from clean surfaces and binary alloys. It is shown that the coincident detection of the electron pair allows for an investigation of the spin-split electronic band structure under the condition of a single binary electron–electron encounter and where the incoherent scattering from the alloy crystal potential is negligible. In general the pair emission can be utilized for studying the electron scattering dynamics in ordered and disordered matter.

References

[1] A. Hubert, R. Schäfer, Magnetic Domains: the Analysis of Magnetic Microstructures, Springer-Verlag, Berlin, 1998.
[2] B. Heinrich, J.A.C. Bland (Eds.), Ultrathin Magnetic Structures, Springer-Verlag, Heidelberg, 1994.
[3] R. Feder (Ed.), Polarized Electrons in Surface Physics, World Scientific, Singapore, 1985.
[4] J. Kirschner, D. Rebenstorff, H. Ibach, Phys. Rev. Lett. 53 (1984) 698;
R. Vollmer, M. Etzkorn, A.P.S. Kumar, H. Ibach, J. Kirschner, Phys. Rev. Lett. 91 (2003) 147201.
[5] D.L. Abraham, H. Hopster, Phys. Rev. Lett. 62 (1989) 1157.
[6] H. Ibach, D.L. Mills, Electron Energy Loss Spectroscopy and Surface Vibrations, Acad. Press, New York, 1982.
[7] J. Berakdar, Phys. Rev. Lett. 83 (1999) 5150.
[8] A. Morozov, J. Berakdar, S.N. Samarin, F.U. Hillebrecht, J. Kirschner, Phys. Rev. B 65 (2002) 104425;
S. Samarin et al., Phys. Rev. Lett. 85 (2000) 1746.
[9] P.J. Durham, J. Phys. F: Metal. Phys. 11 (1981) 2475.
[10] J.S. Faulkner, G.M. Stocks, Phys. Rev. B 21 (1980) 3222.
[11] G.M. Stocks, H. Winter, Z. Phys. B 46 (1982) 95.
[12] B.L. Gyorffy, Phys. Rev. B 5 (1972) 2382.
[13] A. Gonis, Theoretical Materials Science: Tracing the Electronic Origins of Materials Behavior, Materials Research Society, Warrendale, PA, 2000.
[14] I. Turek, V. Drchal, J. Kudrnovský, M. Šob, P. Weinberger, Electronic Structure of Disordered Alloys, Surfaces, and Interfaces, Kluwer Academic Publishers, Boston, 1997.
[15] E. Weigold, I.E. McCarthy, Electron Momentum Spectroscopy, Kluwer Academic/Plenum Publishers, 1999.
[16] S. Iacobucci, L. Marassi, R. Camilloni, S. Nannarone, G. Stefani, Phys. Rev. B 51 (1995) 10252.
[17] K.A. Kouzakov, J. Berakdar, Phys. Rev. B 66 (2002) 235114;
K.A. Kouzakov, J. Berakdar, J. Phys.: Condens. Matter 15 (2003) L41.
[18] J. Berakdar, S.N. Samarin, R. Herrmann, J. Kirschner, Phys. Rev. Lett. 81 (1998) 3535.
[19] R. Feder, H. Gollisch, D. Meinert, T. Scheunemann, O.M. Artamonov, S.N. Samarin, J. Kirschner, Phys. Rev. B 58 (1998) 16418.
[20] W. Kohn, N. Rostoker, Phys. Rev. 94 (1954) 1111.
[21] J. Korringa, Physica 13 (1947) 392.
[22] P. Soven, Coherent-potential model of substitutional disordered alloys, Phys. Rev. 156 (1967) 809.
[23] R.K. Nesbet, Phys. Rev. B 45 (1992) 13234.
[24] D.J. Chadi, M.L. Cohen, Phys. Rev. B 8 (1973) 5747.
[25] J. Berakdar, Surf. Rev. Lett. 7 (2000) 205.